REVIEWS

Journal of Semiconductors
(2023) 44, 103101
doi: 10.1088/1674-4926/44/10/103101

JOS

GaAs-based resonant tunneling diode: Device aspects from design, manufacturing, characterization and applications

Swagata Samanta†

Department of Electronics and Communication Engineering, SRM University-AP, Andhra Pradesh, India

Abstract: This review article discusses the development of gallium arsenide (GaAs)-based resonant tunneling diodes (RTD) since the 1970s. To the best of my knowledge, this article is the first review of GaAs RTD technology which covers different epitaxial-structure design, fabrication techniques, and characterizations for various application areas. It is expected that the details presented here will help the readers to gain a perspective on the previous accomplishments, as well as have an outlook on the current trends and future developments in GaAs RTD research.

Key words: gallium arsenide; microfabrication; resonant tunneling devices

Citation: S Samanta, GaAs-based resonant tunneling diode: Device aspects from design, manufacturing, characterization and applications[J]. *J. Semicond.*, 2023, 44(10), 103101. https://doi.org/10.1088/1674-4926/44/10/103101

1. Introduction

The pioneering work of Leo Esaki and Raphael Tsu[1–3] has led resonant tunneling diode (RTD) to come into recognition. Esaki, during his PhD days (in 1958) reported on a new diode (named the Esaki or tunnel diode) that exhibited negative resistance in its current–voltage (*I*–*V*) characteristic, and which was used for microwave communications, high-frequency amplifier, logic circuits, and oscillators[4–11]. Although this diode was faster than the conventional diodes and transistors, it was hard to use in control circuits, and was also expensive. In 1973, Esaki and Tsu reported a new tunneling phenomenon in a superlattice. It was observed from the computed *I*–*V* characteristic that multibarrier tunneling model would provide better understanding in observing the transport mechanism for a superlattice having limited number of spatial periods or a short mean free path. A year later, in 1974, Chang Tsu and Esaki demonstrated a device based on their previous collaborative work and theories—the RTD. RTD is a semiconductor device that utilizes quantum mechanical tunneling to transport electrons through a thin barrier in the device. The tunneling effect occurs when the energy of the electron is less than the height of the energy barrier, which allows the electron to pass through the barrier without losing any energy. In an RTD, the tunneling effect is enhanced by the presence of a resonant state in the barrier material. This resonant state allows the electrons to tunnel through the barrier more easily, resulting in a peak current that occurs when the energy of the incoming electrons matches the energy of the resonant state. The physics of a RTD can be described by the resonant tunneling mechanism, which involves the coupling of two resonant states in the barrier material. When an electron enters the RTD, it encounters the first resonant state and tunnels through the barrier, entering the quantum-well region of the device. The electron then encounters the second resonant state and tunnels through the second barrier, exiting the device.

RTD typically consists of a quantum well (made from a semiconductor having a smaller bandgap) that is sandwiched between two potential barriers (made from a semiconductor with a larger bandgap). This means that the basic configuration of an RTD is a double-barrier quantum-well (DBQW) structure. When the two-terminal RTD device is biased, electrons having lower kinetic energy than the barriers may tunnel through the DBQW structure. The possibility of electrons tunneling through the barriers is defined by the transmission coefficient. At the resonant state, the transmission coefficient is close to unity. As the transmission coefficient of electrons tunneling through the DBQW changes with the bias voltage, the current–voltage (*I*–*V*) characteristic of the RTD device exhibits negative differential resistance (NDR)[3, 12–14]. The energy band diagram of a typical double-barrier RTD structure and the corresponding *I*–*V* characteristics are shown in Figs. 1 and 2, respectively, where E_c is the conduction band energy, E_f is the Fermi energy, and E_1 and E_2 are the quantization energies; I_p, I_v, V_p, and V_v are the respective peak and valley current and voltages. Fig. 1(a) is the band diagram with no external bias; no current flows in this condition and the quantized states E_1 and E_2 inside the well are larger than the Fermi energy E_f. At small bias voltage (Fig. 1(b)), some current starts flowing through the device as the electrons gain sufficient energy to overcome the barriers. On further increasing the bias voltage and when the electron energy coincides with the quantized state energy E_1 (Fig. 1(c)), resonant tunneling occurs. At resonance (i.e., when the energy levels are equal), there will be more electrons flowing through the barriers and this will result in a peak current I_p. If the bias voltage is increased further, and first resonant energy falls below the conduction band offset (Fig. 1(d)), there will be a sudden drop in current (due to the off-resonance condition) resulting in an NDR regime. The current will continue to drop on further voltage increment (Fig. 1(e)) and will again start rising with increasing voltage when the sec-

Correspondence to: S Samanta, swagata.s@srmap.edu.in
Received 8 FEBRUARY 2023; Revised 10 APRIL 2023.
©2023 Chinese Institute of Electronics

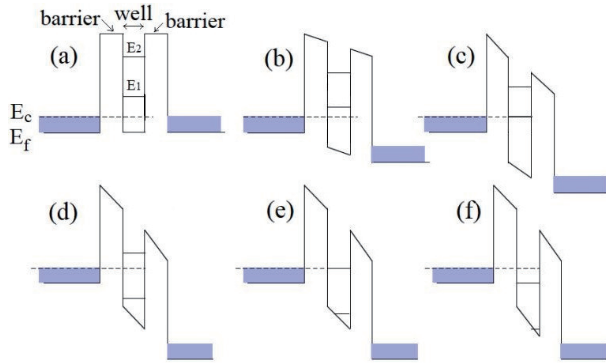

Fig. 1. (Color online) Energy band diagram of a typical double-barrier RTD structure.

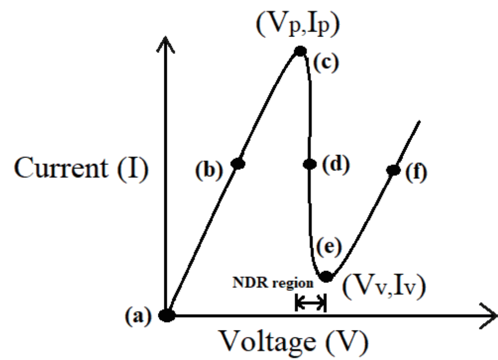

Fig. 2. Corresponding *I*–*V* characteristics of a typical double-barrier RTD structure.

Table 1. Material properties for different semiconductors at room temperature.

Material	Lattice constant (Å)	Electron mobility (cm²/(V·s))	Relative dielectric constant	Energy bandgap (eV)	Electron effective mass (m_0)
Si	5.43095	1500	11.9	1.12 (indirect)	l[1]: 0.98 t: 0.19
Ge	5.64613	3900	16.0	0.66 (indirect)	l: 1.64 t: 0.082
GaAs	5.6533	8500	13.1	1.424 (direct)	0.063
AlAs	5.6605	180	10.1	2.36 (indirect)	0.11
$Al_xGa_{1-x}As$	5.6533 + 0.0078 x	$8 \times 10^3 - 2.2 \times 10^4 x + 10^4 x^2$ (for $0 < x < 0.45$); $-255 + 1160x - 720x^2$ (for $0.45 < x < 1$)	11.96 (when $x = 0.33$)	1.42–2.36 (direct when $x < 0.4$)	$0.063 + 0.083x$ (for $0 < x < 0.45$)
GaP	5.4512	110	11.1	2.26 (indirect)	0.82
GaN	$a = 3.189$ $c = 5.182$	400	10.4	3.44 (direct)	0.27
InP	5.8686	4600	12.6	1.35 (direct)	0.077

[1]where, electron rest mass (m_0) = 9.11×10^{-31} kg; l: longitudinal; t: transverse.

ond resonant energy level falls below the Fermi level energy (Fig. 1(f)).

From Fig. 2, it can be seen that the current–voltage characteristics of an RTD are highly nonlinear, with a NDR region occurring at the peak current. This NDR region is due to the resonant tunneling mechanism, where a small change in the bias voltage can cause a large change in the current flowing through the device.

RTDs have been realized using various semiconductor materials and/or alloy systems, such as group IV (silicon (Si), silicon–germanium (Si–Ge)), and Ⅲ–V compound semiconductors (gallium arsenide (GaAs), indium phosphide (InP), gallium phosphide (GaP), gallium nitride (GaN)). These material systems differ in properties; thus, the choice of material plays a crucial role in the formation of good quality devices. Silicon-based devices are cheap, robust, and easy to process. However, due to their lower electron mobility, they operate more slowly than their Ⅲ–V counterparts. In addition, a wide band gap enables Ⅲ–V based devices to operate at higher temperatures and produce lower thermal noise at room temperature. A list of the properties of these material systems at room temperature[15, 16] is given in Table 1.

Among the RTDs based on Ⅲ–V compound semiconductor material system, GaAs (direct bandgap material) heterostructures were found to be the most prevalent in the early days owing to its high electron mobility. These RTDs con-

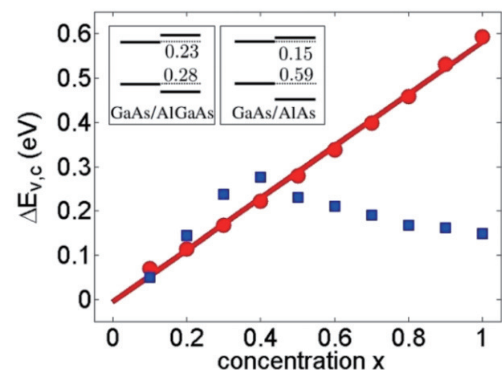

Fig. 3. (Color online) Conduction (blue square) and valence band (red dot) offsets for $Al_xGa_{1-x}As$/GaAs interface with varying aluminum concentration. (Reprinted with permission from Ref. [17]. ©2013 American Institute of Physics.)

sist of a GaAs well sandwiched between AlAs or AlGaAs barriers. The advantage of using this material system is that AlAs and AlGaAs are lattice matched with GaAs, and thus have less material stress. However, the barrier height is low in this material system. This will result in high thermionic emission current, and as a result will be responsible for high valley current at room temperature. The electron effective mass for GaAs/AlGaAs RTDs is high, which reduces the current electron mobility and ultimately results in a decrease in current

density. In addition, these RTDs suffer from low conduction band offset (as depicted in Fig. 3) which produces high leakage currents at the upper resonant level.

The experimental *I–V* characteristics of a double-barrier RTD structure were first observed in 1974[3] and were based on GaAs material technology. Since then, there has been extensive research on the technology, new material systems have been developed, and material growth has been used to obtain high quality RTD devices. Key technologies to obtain high quality RTDs include fabrication technology and structural design. Most of the reported material growth techniques to obtain high-precision ultrathin epi-layers use molecular beam epitaxy (MBE), while only a few use metal organic chemical vapor deposition (MOCVD). This is due to the fact that MBE is more precise and this gives more control of the deposited film thickness, alloy composition, and doping level[18–21].

In this review article, I will cover the development of GaAs RTD technology featuring significant accomplishments that have been achieved in terms of device design, fabrication, characterization, and applications to date. I will also give a research outlook on future developments with this technology. The organization of the article is as follows. Section 2 discusses different epi-structures used in GaAs-based RTDs, fabrication technology and device performances. Section 3 deals with the RTD applications. Finally, future perspectives and concluding remarks are given in Section 4.

2. RTD epi-structure: Device abrication and performance

The simplest RTD epi-structure consists of a quantum well sandwiched between double barriers: A top electrode and a bottom electrode[3]. The dimension of epitaxial layers including barrier thickness, quantum well, and spacer thickness needs to be varied to optimize the device performance, which depends on figure of merits, namely peak to valley current ratio (PVCR) and peak current density (J_p). To have a high PVCR, the peak current (I_p) needs to be as high as possible, while the valley current (I_v) should be as low as possible. However, if the peak current is too high, then it will cause high power dissipation. Consequently, a low peak voltage RTD needs to be designed in order to equilibrate this. Peak current density is inversely related to the barrier thickness—as barrier thickness decreases, it enlarges the transmission probability, which finally results in an increment of current density[22]. The distance between the adjacent resonant energy levels will increase if the quantum well is made narrow, so the leakage current components through the second resonant energy level will reduce, which ultimately enhances the PVCR[23–26]. The addition of a spacer layer in the RTD epi-structure prevents dopant diffusion to the subsequent layer in the growth process. However, a thick spacer layer widens the depletion region, which will affect high-frequency device performance by increasing the intrinsic delay time. It has also been found that introducing a spacer will result in an increase in the operating voltage. Furthermore, in specific designs, it has been shown that introducing doping in the active region can boost the performance of the device by altering the energy band structure and enhancing its current–voltage properties. In particular, doping can affect the tunneling current that flows through the RTD's active region[27–30].

High-frequency RTD device fabrication can be carried out by using one of the three processes, namely, a) Polyimide process[31], b) Air-bridge process[32, 33], and c) BCB (benzocyclobutene) process[34]. Processing steps in general involve sample cleaning, lithography, etching, and metallization. In the polyimide RTD process, the first fabrication step is the formation of top metal contact. Next is the top mesa step, which will etch till the emitter layer (using proper etching solution as depicted in Table 3). The bottom metal contact is deposited then following the same procedure as the top metal. The next step of fabrication is the bottom mesa, which etches till the substrate. This step isolates the active layers from the surrounding areas. The passivation step is done by using a polyimide (e.g., PI 2545), and thereafter the via-opening step is to be carried out in order to enable a connection between top contact and bond pads. Finally, metal bond pads are formed, which completes the single RTD device fabrication process. Figs. 4 and 5 show the RTD fabrication flow by using polyimide process and SEM (scanning electron microscope) image after fabrication, respectively.

The via-opening step, although crucial, is a critical process of RTD device fabrication, where a slight misalignment of mask and improper etch (underetch/overetch) may even result in device failure. In addition, creating a via-hole becomes very challenging when mesa size is of nanoscale dimension. This can be overcome with the air-bridge approach or by BCB process. RTD fabrication with air-bridge approach starts with top metal contact formation and mesa definition (which etches down to the emitter layer). Following this is a second etch step similar to the mesa step which results in a suspended air-bridge structure. Finally, there is bottom contact formation and bond pad establishment step. Thus, the air-bridge builds a connection between top metal and bond pad, thereby eliminating the critical via-opening step of polyimide process. The SEM image and actual micrograph of a GaAs/AlAs RTD device fabricated by the air-bridge process as reported by Zawawi[32] is shown in Fig. 6.

Fabrication of RTD using BCB process starts with the top metal formation, top mesa, bottom metal formation, bottom mesa step, and passivation similar to the polyimide process. However, after this passivation, there is no via-opening. In this case, BCB etch back process to etch till top metal is undertaken and then bottom contact opening is done; finally, the bond pads are established. The cross-sectional view after the bond pad step is shown in Fig. 7.

A suitable ohmic contact metallization scheme needs to be chosen for the fabrication of RTD, which will be thermally stable and have low contact resistance (R_c). These two are very important criteria for the performance and reliability of any semiconductor device, including the RTD. Ohmic contacts in general provide a link between external circuit and active regions of semiconductor devices. The choice of ohmic contact metallization becomes even more critical for devices with dimensions in the sub-micrometer range. Generally, ohmic contacts for GaAs are deposited by either evaporation or sputtering techniques, and the contact resistances are measured by using transmission line model (TLM). Table 2 shows the state-of-the-art methods and materials for obtaining ohmic contacts to GaAs.

Optical lithography using chrome/glass mask is the most

Fig. 4. (Color online) RTD device fabrication flow by polyimide process: (a) top metal deposition; (b) top mesa; (c) bottom metal deposition; (d) bottom mesa; (e) passivation and via-opening; and (f) bond pad formation.

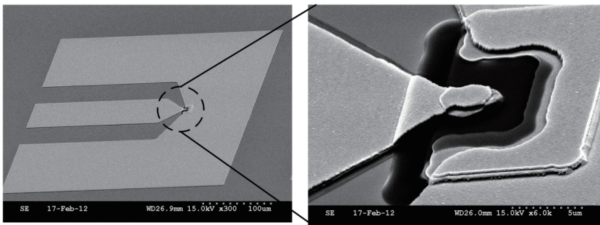

Fig. 5. SEM image of a fabricated RTD device with 3 × 3 μm² mesa area. (Reprinted with permission from Ref. [31]. ©2014 University of Glasgow.)

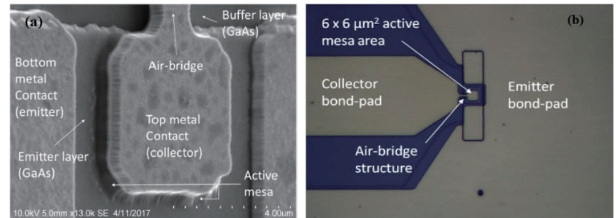

Fig. 6. (Color online) (a) SEM image and (b) actual micrograph of a GaAs/AlAs RTD device fabricated by air-bridge process. (Reprinted with permission from Ref. [32]. ©2017 Elsevier.)

commonly used approach to fabricate a GaAs-based RTD device. This method is inexpensive, and provides adequate resolution and high throughput when compared to the well-known maskless lithography technique—electron beam lithography. As device manufacturing using photolithography often requires wet etching, the next focus would be on the chemical wet etching solution. Etchant composition, concentration, and processing temperature are the crucial factors that

Table 2. Ohmic contact formation on GaAs substrate.

Metal scheme	Deposition method	Anneal temperature (°C)	Anneal time (s)	Specific contact resistance (Ω·cm^2)	Ref.
Pd/Ge/Pd	EB-PVD	430	15	3.2×10^{-4}	[35]
Pd/Ge/Ti/Pt	EB-PVD	430	15	8×10^{-7}	[35]
Pd/Ge/Pd/Ti/Au	EB-PVD	415	15	4.3×10^{-7}	[35]
Pd/Sn	Resistance-heating evaporation	360	1800	3.26×10^{-5}	[36]
Pd/Ge/Ti/Au	EB-PVD	340	20	2.8×10^{-6}	[37]
Pd/Ge/Ti/Pt	EB-PVD	380–450	20	$(2.4–5.3) \times 10^{-6}$	[38]
Pd/Ge/Au/Pd/Au	EB-PVD	400	30	2×10^{-6}	[39]
Pd/Ge/Au/Pd/Au	EB-PVD	320 initially, then 400	20, then 60	2×10^{-6}	[40]
Au/Ge/Ni/Au	EB-PVD	400	60	5.6×10^{-6}	[41]
Ge/Cu	EB-PVD	400	1800	7×10^{-7}	[42]
Ge/Au/Ni/Ta/Au	Magnetron sputtering	450	–	7×10^{-7}	[43]
WSi/Cu	RF sputtering	400	5	6.3×10^{-6}	[44]
Au/Ti/W/Ti	Sputtering and EB-PVD	400	30	5.5×10^{-6}	[45]
In	IAD	375	60	3×10^{-6}	[46]

where, EB-PVD: electron beam physical vapor deposition; RF: radio frequency; resistance-heating evaporation: resistive evaporation; IAD: ion-assisted deposition.

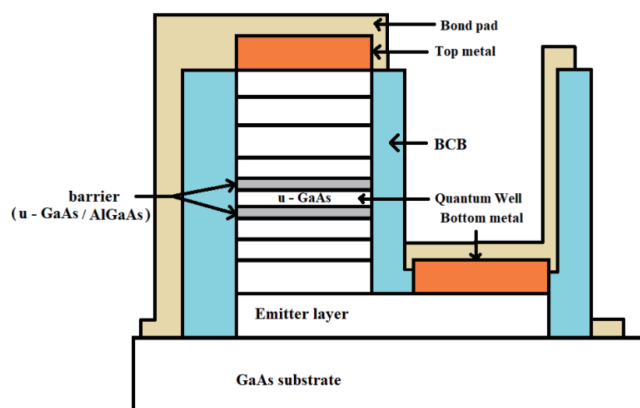

Fig. 7. (Color online) Cross section after bond pad establishment for BCB process of RTD fabrication.

affect the etching profile. Table 3 illustrates the state-of-the-art wet etchants for GaAs material around room temperature. The etchants are based on ammonium hydroxide, hydrochloric-based, sulfuric-based, orthophosphoric, or citric acid-based etching solutions. Although the wet etch method has the advantage of being low cost, it causes low damage to surface, and provides high selectivity, a dry etch method is also required where the main concern is to obtain high resolution and vertical sidewalls. Table 4 provides details of dry etching for GaAs material.

There are intense research efforts to optimize the performance of RTDs to be utilized as building blocks of electronics, as well as optical devices. Presently, fabrication demands maximum performance with minimum device size. However, scaling down device size increases the on-chip device density and decreases the capacitance, which ultimately lowers the cut-off operating frequency[63]. Table 5 shows the state-of-the-art performance of GaAs-based RTDs in terms of PVCR and peak current density at room temperature. Generally, a parameter analyzer is used to measure the RTD DC characteristics, where the bond pads are connected to the terminals on the parameter analyzer through two DC probes, and measurement software is used to manage measurement and enable data collection. It can be observed from Table 5 that a proper choice of material system, thereby adjusting the doping concentration of contact regions, will help to improve the performance of RTD structures. The dimensions of the individual layers forming the RTD device (i.e., barrier, well and spacer thicknesses) also play important role in performance improvement.

3. Application

Resonant tunneling diodes exhibit a wide variety of applications in electronics and communication systems, including high-speed digital circuits, microwave oscillators, terahertz detectors, and optical applications (Table 6). The unique properties of RTDs, such as their high-frequency response and low power consumption, make them an attractive choice for these applications. RTDs are known to be the fastest semiconductor-based electronic devices to date[81, 82]. Tunneling time and device capacitance are very small in these devices, which makes their operation frequency and switching speed the fastest when compared to other semiconductor-based electronic devices, and are thus used in high-frequency electronics. With a higher peak current density, RTDs will have faster switching speed, provided that the PVCR is kept high and the device capacitance is kept low. RTD can potentially operate in the terahertz (THz) regime because it is only limited by tunneling time of the electrons, which is in the order of picoseconds. The NDR allows fast oscillations, so oscillators can be made that will oscillate at THz. This NDR also allows RTD to be applicable in digital logic circuits[83]. One can make the RTD oscillate at very high frequency with a small device capacitance and small intrinsic delay. In 1984, Sollner[84] reported the first demonstration of GaAs/AlGaAs RTD oscillator at an oscillation frequency of 18 GHz at 200 K temperature. Oscillators operating at room temperature were reported later by Brown[64–66] for GaAs/AlAs RTDs, and could work up to 420 GHz[66]. Operation of the RTD as both oscillator and detector is possible by changing the operation bias voltage, and there-

Table 3. Wet etching solution for GaAs material around room temperature.

Etching solution	Etchant ratio	Temperature (°C)	Etch rate (nm/min)	Ref.
$NH_4OH : H_2O_2 : H_2O$	1 : 1 : 25	25	924	[47]
	1 : 1 : 50		594	
	1 : 2 : 50		861	
	2 : 1 : 50		993	
	1 : 1 : 250		177	
	1 : 1 : 500		54	
	40 : 4 : 1	Room temp.	202.6	[48]
	40 : 10 : 0		509.1	
	40 : 20 : 0		1385	
	1 : 1 : 5		1890	
	1 : 10 : 500		25	
	10 : 1 : 500		18	
	1 : 10 : 5000		6.1	
	1 : 1 : 5000		1.65	
	1 : 10 : 3000		12	
$HCl : H_3PO_4 : H_2O$	1 : 10 : 1	20	10	[49]
$HCl : CH_3COOH : H_2O$	1 : 10 : 1	20	60	[49]
$HCl : CH_3COOH : H_2O_2$	1 : 20 : 0	20	10	[50]
	1 : 20 : 1		50	
	1 : 20 : 2		120	
	1 : 20 : 3		270	
	1 : 2 : 1		440	
	1 : 5 : 1		250	
	1 : 10 : 1		120	
	1 : 20 : 1		50	
	1 : 30 : 1		30	
	1 : 40 : 1		15	
$H_3PO_4 : H_2O_2 : H_2O$	3 : 1 : 50	Room temp.	60	[32]
	3 : 1 : 75	Room temp.	72	[51]
	1 : 1 : 25	25	259.8	[47]
	1 : 1 : 50		130.8	
	1 : 2 : 50		244.8	
	2 : 1 : 50		129	
	1 : 1 : 250		40.8	
	1 : 1 : 500		7.8	
$H_3PO_4 : HNO_3$	3 : 1	Room temp.	1125	[48]
$H_2SO_4 : H_2O_2$	4 : 1	Room temp.	1073	[48]
$H_2SO_4 : H_2O_2 : H_2O$	4 : 3 : 3	Room temp.	9000	[52]
	1 : 1 : 25	25	234	[47]
	1 : 1 : 50		90.6	
	1 : 2 : 50		202.8	
	2 : 1 : 50		184.8	
	1 : 1 : 250		27	
	1 : 1 : 500		27.6	
$C_6H_8O_7 : H_2O_2$	2 : 1	20	30	[53]
	3 : 1		45	
	4 : 1		45	
	5 : 1		42	
	7 : 1		33	
	10 : 1		21	
	1 : 1	18	5	[54]
	1 : 3		7	
	1 : 5		200	
	1 : 10		210	
	1 : 15		150	
	1 : 25		90	
	1 : 1	21	5.8	[55]
	2 : 1		570	

Table 3. (Continued)

Etching solution	Etchant ratio	Temperature (°C)	Etch rate (nm/min)	Ref.
$HCl : HNO_3$	3 : 1	Room temp.	477	[48]
$HCl : HNO_3 : H_2O$	1 : 1 : 1	Room temp.	2277	[48]
$HCl : H_2O_2 : H_2O$	1 : 10 : 500	Room temp.	9.27	[48]
	80 : 4 : 1		185	
	1 : 10 : 5000		8.21	
$HF : HNO_3 : H_2O$	1 : 1 : 1	Room temp.	122693	[48]

Table 4. Dry etching details for GaAs material.

Inductively coupled plasma etching						
Gas system	Flow rate (sccm)	RF power (W)	ICP power (W)	Chamber pressure (mTorr)	Etch rate (μm/min)	Ref.
BCl_3/Cl_2	30/80	80	600	10	2.6	[56]
			800		4.5	
			1000		5.4	
			1200		6.2	
			1500		6.4	
			600	5	3.2	
				10	2.8	
				15	1.8	
				20	1.2	
		150		10	3.6	
		200			4.0	
		300			4.4	
BCl_3/Cl_2	3 : 4 (ratio)	90	950	40	~4.0	[57]
BCl_3/Cl_2	4 : 1	RF : ICP = 1 : 8		10	3.64	[58]
	2 : 1				3.6	
	2.5 : 1				2.38	
	6 : 1				2.37	
	8 : 1				2.1	
$BCl_3/Cl_2/Ar$	4 : 1 : 5	RF : ICP = 1 : 8		10	2.38	[58]
	2.5 : 1 : 5				2.13	
	6 : 1 : 5				2.0	
$BCl_3/Cl_2/Ar/N_2$	6 : 1 : 5 : 2	RF : ICP = 1 : 8		10	3.84	[58]
	6 : 1 : 5 : 2.5				4.0	
	6 : 1 : 5 : 3				4.0	
	3 : 1 : 5 : 3				2.5	
	20 : 1 : 5 : 3				1.8	
				5	1.14	
				20	2.36	
				25	3.6	
				30	3.7	
	20 : 1:5 : 5			30	5.56	
				20	4.1	
	20 : 1 : 10 : 3			20	2.8	
	20 : 1 : 20 : 3				3.0	
	20 : 1 : 30 : 3				2.5	
	20 : 1 : 50 : 3				2.23	
$BCl_3/Cl_2/N_2$	20 : 1 : 3	RF : ICP = 1 : 8		10	1.92	[58]
Cl_2/Ar	13/20	80	250	7.5	1.37	[59]
		150			1.6	
		200			1.82	
$Cl_2/Ar/SiCl_4$	13/20/5	150	250	7.5	1.65	

Table 4. (Continued)

Reactive ion etching					
Gas system	Flow rate (sccm)	RF power (W)	Chamber pressure (mTorr)	Etch rate (μm/min)	Ref.
CCl_4/CCl_2F_2	1/5	200	40	1.3	[57]
CCl_2F_2/He	10/15	85	10	0.2	[60]
			20	0.5	
			30	0.7	
			40	1.05	
			50	1.3	
			60	1.4	
$SiCl_4$/Ar	5/10	20	30	0.75	[61]
		30		1.25	
		50		1.25	
		30	50	1.5	
			80	2.5	
$SF_6/(BCl_3 + SF_6)$	1 : 5	150	50	1.8	[62]
	2 : 5			4.2	
	11 : 20			5.5	
	3 : 5			2.7	
	4 : 5			4.5	
CCl_2F_2/Ar	1 : 10	200	200	0.32	[33]
			300	0.23	
			400	0.15	
			500	0.08	
			600	0.15	

fore RTDs can be used in realization of compact and low-cost transceivers. Research has also been done for RTD photodetectors (PD) on GaAs substrates (GaAs/AlGaAs RTD PD) by the inclusion of quaternary absorption layer like GaInNAs, which is pseudomorphically grown on GaAs substrates[85]. In order to enable wavelength-selective detection and enhance the quantum efficiency, RTDs are often integrated with distributed Bragg reflector (DBR) cavity[86, 87]. Sensitivity and wavelength selectivity depends on the number of DBR mirror pairs used—increasing the mirror pairs enhances both sensitivity and wavelength selectivity. The detection efficiency can also be enhanced with integrated waveguide geometry, as reported by Pfenning[87], where the waveguide design was for a wavelength of 940 nm. Effort has also been made to make use of RTDs as pressure sensors[88], mixers[77], and in trigger circuits[79].

4. Conclusions and future perspectives

RTDs have become a research focus due to their NDR current–voltage characteristics, structural simplicity, low fabrication cost, inherent high speed, design flexibility, versatile circuit functionality, and ability to operate at room temperature. NDR is the reason why RTDs have found potential for high-speed and high functionality operations, thus gaining the attention to researchers working in this field. Researchers and scientists from different parts of the world have been working with RTDs using GaAs material system to make them applicable for a wide range of applications. The advent of various advanced epitaxial growth techniques and fabrication methods makes it possible to improve the performance and allows them to be applied in many areas. However, there is much research space for the development of this GaAs RTD technology. In particular, much optimization is required to make it potential for real-world applications, especially in terahertz and neuromorphic applications. In recent years, there has been a trend of developing RTD devices in brain-inspired optical memories and neuromorphic computing. Neuromorphic electronic circuits that are based on optoelectronic devices are formed by RTDs to enable electro-optic neuromorphic functions. It is highly expected that in the near future the research focus would be on the implementation of neuromorphic applications using GaAs-based RTDs.

Table 5. Performance of GaAs-based RTDs at room temperature.

Material system		PVCR	J_p (kA/cm^2)	Mesa size	Ref.
Barrier (nm)	Well (nm)				
AlAs (1.7)	GaAs (4.5)	3.5	40	–	[64]
$Al_{0.3}Ga_{0.7}As$ (3.0)	GaAs (4.5)	1.3	12	–	[65]
AlAs (2.5)	GaAs (4.5)	1.7	8	–	
AlAs (1.5)	GaAs (4.5)	3.5	40	–	
AlAs (1.1)	GaAs (4.5)	1.5	150	Φ = 4 μm	[66]
$Al_{0.3}Ga_{0.7}As$ (5.0)	GaAs (5.0)	1.8	30	177 μm^2 (Φ = 15 μm)	[67]
AlAs (1.7)	GaAs (5.0)	4.1 ± 0.1	48.8 ± 3.8	–	[68]
		3.8 ± 0.2	52.2 ± 2.2	–	
AlAs (1.7)	GaAs (4.5)	2.0	160	Φ = 3.5 μm	[69]
AlAs (1.4)	GaAs (5.1)	1.8	250 ± 20	(1–3) × 5 μm^2	[70]
AlAs (1.7)	GaAs (4.5)	2.0	140 ± 10		
AlAs (1.4)	GaAs (4.5)	1.7	200 ± 20		
AlAs (1.7)	GaAs (4.5)	5.0	35	49	[71]
AlAs (1.7)	GaAs (5.0)	4.8	8.3	36	[72]
AlAs (4.0)	GaAs (5.5)	1.45	–	900	[73]
AlAs (2.0)	GaAs (5.0)	4.1	13.3	49	[74]
		5.0	14.7		
$Al_{0.42}Ga_{0.58}As$ (5.0)	GaAs (5.0)	3.9	0.61	520	[75]
$Al_{0.42}Ga_{0.58}As$ (1.7)	GaAs (5.0)	5.35	40	>16	[76]
AlAs (1.7)	GaAs (4.0)	2.9	6	100	[77]
AlAs (4.0)	GaAs (4.7)	2.9	2	2500	[78]
		1.7	1.53	7500	
AlAs (1.7)	GaAs (4.5)	3.5	100	12	[79]
AlAs (1.96)	GaAs (5.0)	4.0	20	75	[80]
AlAs (1.7)	GaAs (6.5)	3.27	14.8	16	[32]
		3.44	15.93	25	
		3.38	14.8	36	

References

[1] Esaki L, Tsu R. Superlattice and negative differential conductivity in semiconductors. IBM J Res Dev, 1970, 14, 61

[2] Tsu R, Esaki L. Tunneling in a finite superlattice. Appl Phys Lett, 1973, 22, 562

[3] Chang L L, Esaki L, Tsu R. Resonant tunneling in semiconductor double barriers. Appl Phys Lett, 1974, 24, 593

[4] Hall R N. Tunnel diodes. IRE Trans Electron Devices, 1960, 7, 1

[5] Sommers H S. Tunnel diodes as high-frequency devices. Proc IRE, 1959, 47, 1201

[6] Sterzer F, Nelson D. Tunnel-diode microwave oscillators. Proc IRE,

Table 6. Applications of GaAs-based RTDs.

RTD as oscillator					
Material system	Operation frequency (GHz)	Temperature (K)		Output power (μW)	Ref.
GaAs/AlGaAs	18	200		0.5	[84]
GaAs/AlAs	200 60 3 0.2	300		20 60 100 200	[64]
GaAs/AlAs	56 87	300		60 18	[65]
GaAs/AlAs	3 12 50 100 220 350 420	300		150 150 50 25 2 0.2 0.2	[66]
GaAs/AlGaAs	2 to 12	300		–	[67]
GaAs/AlAs	38.6 110	300		36 12	[69]
RTD as photodetector/light sensor and in single photon detection					
Device scheme	Wavelength (μm)	Voltage (V)	Absorption (%)	Sensitivity (kA/W)	Ref.
RTD with absorption layer	1.3	3.0	–	0.966	[85]
RTD integrated into DBR cavity	1.29	4.0	18.3	31.2	[86]
RTD integrated into DBR cavity	0.94	–	90	–	[87]
Waveguide-integrated RTD	0.94	–	>90 (max 99)	–	[87]
RTD as pressure sensor					
Material system	Frequency (kHz)		Sensitivity (kHz/MPa)		Ref.
GaAs/AlGaAs	113		0.8		[88]
RTD as switch					
Material system	Switching time (ps)		Voltage swing (mV)		Ref.
GaAs/AlAs	20		60		[80]
RTD as subharmonic mixer					
Material system	Threshold voltage for resonant tunneling (V)	Temperature (K)	Local oscillation power (dBm)	Conversion loss (dB)	Ref.
GaAs/AlAs	0.75	Room temp.	12	11	[77]
RTD in triggering					
Material system	Frequency range (GHz)	Time jitter (ps·rms)		Bandwidth (GHz)	Ref.
GaAs/AlAs	5 to 50	<1		60	[79]

1961, 49, 744

[7] Burrus C A. Gallium arsenide Esaki diodes for high-frequency applications. J Appl Phys, 1961, 32, 1031

[8] Greene J C, Sard E W. Experimental tunnel-diode mixer. Proc IRE, 1961, 49, 350

[9] Robertson W J. A broadband hybrid coupled tunnel diode down converter. Proc IRE, 1960, 48, 2023

[10] Reindel J. Tunnel diode circuits at nicrowave frequencies. 1961. Available: https://apps.dtic.mil/dtic/tr/fulltext/u2/269846.pdf

[11] Bessho T, Hiyama Y, Niiyama H. Memory circuit using Esaki diode. Review of the Electrical Communication Laboratory, Tokyo, 1969, 17, 89

[12] Roblin P, Rohdin H. High-speed heterostructure devices: From device concepts to circuit modeling. Cambridge: Cambridge University Press, 2002

[13] Mizuta H, Tanoue T. The physics and applications of resonant tunnelling diodes. Cambridge: Cambridge University Press, 1995

[14] Figueiredo J M L. Optoelectronic properties of resonant tunnelling diodes. Ph.D. Dissertation, University of Glasgow, 2000

[15] Dobson P. Physics of semiconductor devices (2nd ed.). Phys Bull, 1982

[16] Levinshtein M. Handbook series on semiconductor parameters: vol. 2 Ternary and quaternary III-V compounds. World Scientific, 1996

[17] Wang Y, Zahid F, Zhu Y, et al. Publisher's Note: Band offset of GaAs/$Al_xGa_{1-x}As$ heterojunctions from atomistic first principles [Appl. Phys. Lett. 102, 132109 (2013)]. Appl Phys Lett, 2013, 103, 049901

[18] Campbell A C, Kesan V P, Block T R, et al. Influence of MBE growth temperature on GaAs/AlAs resonant tunneling structures. J Electron Mater, 1989, 18, 585

[19] Nishiwaki T, Yamaguchi M, Sawaki N. AlGaAs/GaAs nano-hetero-

epitaxy on a patterned GaAs substrate by MBE. AIP Conference Proceedings, Vienna (Austria), 2007, 893, 61

[20] Kapre R, Madhukar A, Kaviani K, et al. Realization and analysis of GaAs/AlAs/$In_{0.1}Ga_{0.9}As$ based resonant tunneling diodes with high peak-to-valley ratios at room temperature. Appl Phys Lett, 1990, 56, 922

[21] Koenig E T, Jogai B, Paulus M J, et al. Charge-quantization effects on current–voltage characteristics of AlGaAs/GaAs resonant tunneling diodes with spacer layers. J Appl Phys, 1990, 68, 3425

[22] Kim S K, Kang T W, Kim T W. Electrical transport properties of AlAs/GaAs resonant tunneling diodes. Phys Status Solidi A, 1993, 140, K17

[23] Schmidt T, Tewordt M, Haug R J, et al. Peak-to-valley ratio of small resonant-tunneling diodes with various barrier-thickness asymmetries. Appl Phys Lett, 1996, 68, 838

[24] Tsuchiya M, Sakaki H. Dependence of resonant tunneling current on well widths in AlAs/GaAs/AlAs double barrier diode structures. Appl Phys Lett, 1986, 49, 88

[25] Su B, Goldman V J, Cunningham J E. Single-electron tunneling in nanometer-scale double-barrier heterostructure devices. Phys Rev B, 1992, 46, 7644

[26] Goldman V J, Tsui D C, Cunningham J E. Observation of intrinsic bistability in resonant tunneling structures. Phys Rev Lett, 1987, 58, 1256

[27] Wei T, Stapleton S. Effect of spacer layers on capacitance of resonant tunneling diodes. J Appl Phys, 1994, 76, 1287

[28] Mehdi I, Mains R K, Haddad G I. Effect of spacer layer thickness on the static characteristics of resonant tunneling diodes. Appl Phys Lett, 1990, 57, 899

[29] Singh M M, Siddiqui M J, Khan A B, et al. Effect of barriers length and doping concentration on GaAs/AlGaAs RTD. 2015 Annual IEEE India Conference (INDICON), 2016, 1

[30] Singh M M, Siddiqui M J, Khan A B, et al. Simulation study of I–V characteristics of RTD with variation in doping concentration. IMPACT-2013, 2013, 260

[31] Wang J. Monolithic microwave/millimetre wave integrated circuit resonant tunnelling diode sources with around a milliwatt output power, Ph.D. Thesis, University of Glasgow, 2014

[32] Md Zawawi M A, Missous M. Design and fabrication of low power GaAs/AlAs resonant tunneling diodes. Solid-State Electron, 2017, 138, 30

[33] Dultsev F N, Nenasheva L A. The effect of hydrogen as an additive in reactive ion etching of GaAs for obtaining polished surface. Appl Surf Sci, 2006, 253, 1287

[34] Wang J, Alharbi K, Khalid A, et al. Planar fabrication process development for mm-wave resonant tunneling diode (RTD) using BCB etch-back. 27th International Conference on Indium Phosphide and Related Materials, 2015

[35] Ivey D G, Eicher S, Wingar S, et al. Performance of Pd–Ge based ohmic contacts to n-type GaAs. J Mater Sci Mater Electron, 1997, 8, 63

[36] Islam M S, McNally P J, Cameron D C, et al. Properties of Pd/Sn ohmic contacts on n-GaAs. J Mater Process Technol, 1998, 77, 42

[37] Kwak J S, Baik H K, Lee J L, et al. A low-resistance Pd/Ge/Ti/Au ohmic contact to a high-low doped GaAs field-effect transistor. Thin Solid Films, 1996, 290/291, 497

[38] Lim J W, Mun J K, Nam S, et al. PdGe-based ohmic contacts to high-low doped n-GaAs with and without undoped cap layer. J Phys D: Appl Phys, 2000, 33, 1611

[39] Lim J W, Mun J K, Kwak M H, et al. Performance of Pd/Ge/Au/Pd/Au ohmic contacts and its application to GaAs metal-semiconductor field-effect transistors. Solid-State Electron, 1999, 43, 1893

[40] Papageorgiou V. Integration of planar Gunn diodes and HEMTs for high-power MMIC oscillators. Ph.D. Thesis, University of Glasgow, 2014

[41] Lin H C, Senanayake S, Cheng K Y, et al. Optimization of AuGe-Ni-Au ohmic contacts for GaAs MOSFETs. IEEE Trans Electron Devices, 2003, 50, 880

[42] Aboelfotoh M O, Oktyabrsky S, Narayan J, et al. Electrical and microstructural characteristics of Ge/Cu ohmic contacts to n-type GaAs. J Mater Res, 1997, 12, 2325

[43] Erofeev E V, Loshchilov A G, Tomashevich A A, et al. Low resistance ohmic contacts to n^+ -GaAs with refractory metal sidewall diffusion barrier. International J Civil Engg Technol, 2018, 9, 994

[44] Oku T, Furumai M, Uchibori C J, et al. Formation of WSi-based ohmic contacts to n-type GaAs. Thin Solid Films, 1997, 300, 218

[45] Zhou J, Xia G Q, Li B H, et al. Electrical and structural properties of refractory metal multilayer Au/Ti/W/Ti ohmic contacts to n-GaAs. Jpn J Appl Phys, 2003, 42, 2609

[46] Davies D W, Morgan D V, Thomas H. Indium-based ohmic contacts to n-GaAs, fabricated using an ion-assisted deposition technique. Semicond Sci Technol, 1999, 14, 615

[47] Guan L H, Yusof A, Dolah A, et al. The etching of GaAs, AlGaAs and InGaAs in different chemicals in p-HEMT mesa layers. 2004 IEEE International Conference on Semiconductor Electronics, 2006, 1

[48] Sioncke S, Brunco D P, Meuris M, et al. Etch rates of Ge, GaAs and InGaAs in acids, bases and peroxide based mixtures. ECS Trans, 2008, 16, 451

[49] Skriniarova J, Kovac J, Breza J, et al. Wet etching of InGaP and GaAs in HCl: H_3PO_4: H_2O_2. Sensors and Materials, 1998, 10, 213

[50] Flemish J R, Jones K A. Selective wet etching of GaInP, GaAs, and InP in solutions of HCl, CH_3COOH , and H_2O_2. J Electrochem Soc, 1993, 140, 844

[51] Noda T, Mitsuishi K, Mano T. Fabrication of submicron GaAs/AlAs double-barrier resonant tunneling diodes by wet etching with in droplets as mask. Jpn J Appl Phys, 2007, 46, L994

[52] Fobelets K, Vounckx R, Borghs G. A GaAs pressure sensor based on resonant tunnelling diodes. J Micromech Microeng, 1994, 4, 123

[53] Lee H J, Tse M S, Radhakrishnan K, et al. Selective wet etching of a heterostructure with citric acid-hydrogen peroxide solutions for pseudomorphic GaAs/$Al_xGa_{1-x}As$/$InyGa_{1-y}As$ heterojunction field effect transister fabrication. Mater Sci Eng B, 1995, 35, 230

[54] Juang C. Selective etching of GaAs and $Al_{0.30}Ga_{0.70}As$ with citric acid/hydrogen peroxide solutions. J Vac Sci Technol B, 1990, 8, 1122

[55] Hays D C. Selective etching of compound semiconductors. Master of Science Thesis, University of Florida, 1999

[56] Wang H L, Guo X, Shen G D. GaAs backside via-hole etching using ICP system. Sci China Ser E-Technol Sci, 2007, 50, 749

[57] Rawal D, Agarwal V, Sharma H, et al. Dry etching of GaAs to fabricate via-hole grounds in monolithic microwave integrated circuits. Def Sci J, 2009, 59, 363

[58] Vigneron P B, Joint F, Isac N, et al. Advanced and reliable GaAs/AlGaAs ICP-DRIE etching for optoelectronic, microelectronic and microsystem applications. Microelectron Eng, 2018, 202, 42

[59] Booker K, Mayon Y O, Jones C, et al. Deep, vertical etching for GaAs using inductively coupled plasma/reactive ion etching. J Vac Sci Technol B, 2020, 38, 012206

[60] Chang E Y, Van Hove J M, Pande K P. A selective dry-etch technique for GaAs MESFET gate recessing. IEEE Trans Electron Devices, 1988, 35, 1580

[61] Lujan A S, Ramos A C S, Swart J W. Reactive ion etching of GaAs using $SiCl_4$/Ar. Unicamp, Sau Paulo, Brazil, Available: https://www.ipen.br/biblioteca/cd/cbms/1997/SBMicro/ARTIGO34.PDF

[62] Lee Y S, Upadhyaya K, Nordheden K J, et al. Selective reactive ion etching of GaAs/AlAs in BCl_3/SF_6 for gate recess. J Vac Sci Technol B, 2000, 18, 2505

[63] Liu H C, Sollner T C L G. High-frequency resonant-tunneling devices. In: Semiconductors and semimetals. Elsevier, 1994

[64] Brown E R, Goodhue W D, Sollner T C L G. Fundamental oscillations up to 200 GHz in resonant tunneling diodes and new estimates of their maximum oscillation frequency from stationary-state tunneling theory. J Appl Phys, 1988, 64, 1519
[65] Brown E R, Sollner T C L G, Goodhue W D, et al. Millimeter-band oscillations based on resonant tunneling in a double-barrier diode at room temperature. Appl Phys Lett, 1987, 50, 83
[66] Brown E R, Sollner T C L G, Parker C D, et al. Oscillations up to 420 GHz in GaAs/AlAs resonant tunneling diodes. Appl Phys Lett, 1989, 55, 1777
[67] Bouregba R, Vanbesien O, Saint de Pol L, et al. $Al_{0.3}Ga_{0.7}As$-GaAs microwave resonant tunneling oscillator. Ann Télécommun, 1990, 45, 184
[68] Tsao A. AlAs/GaAs Double barrier resonant tunneling diodes. Ph.D. Thesis, Chapter 4, University of Texas at Austin, 1993, 45
[69] Bouregba R, Vanbesien O, Mounaix P, et al. Resonant tunneling diodes as sources for millimeter and submillimeter wavelengths. IEEE Trans Microwave Theory Techn, 1993, 41, 2025
[70] Wolak E, Özbay E, Park B G, et al. The design of GaAs/AlAs resonant tunneling diodes with peak current densities over 2×10^5A cm^{-2}. J Appl Phys, 1991, 69, 3345
[71] Wei T, Stapleton S, Berolo O. Capacitance and hysteresis study of AlAs/GaAs resonant tunneling diode with asymmetric spacer layers. J Appl Phys, 1995, 77, 4071
[72] Huang Y L, Ma L, Yang F H, et al. Resonant tunnelling diodes and high electron mobility transistors integrated on GaAs substrates. Chin Phys Lett, 2006, 23, 697
[73] Van Hoof C, Genoe J, Mertens R, et al. Electroluminescence from bipolar resonant tunneling diodes. Appl Phys Lett, 1992, 60, 77
[74] Cheng P, Harris J S Jr. Improved design of AlAs/GaAs resonant tunneling diodes. Appl Phys Lett, 1990, 56, 1676
[75] Huang C I, Paulus M J, Bozada C A, et al. AlGaAs/GaAs double barrier diodes with high peak-to-valley current ratio. Appl Phys Lett, 1987, 51, 121
[76] Forster A, Lange J, Gerthsen D, et al. The effect of growth temperature on AlAs/GaAs resonant tunnelling diodes. J Phys D: Appl Phys, 1994, 27, 175
[77] Alkeev N V, Averin S V, Dorofeev A A, et al. GaAs/AlAs resonant-tunneling diode for subharmonic mixers. Russ Microelectron, 2010, 39, 331
[78] Kan S C, Wu S, Sanders S, et al. Optically controlled resonant tunneling in a double-barrier diode. J Appl Phys, 1991, 69, 3384
[79] Yang L, Draving S D, Mars D E, et al. A 50 GHz broad-band monolithic GaAs/AlAs resonant tunneling diode trigger circuit. IEEE J Solid-State Circuits, 1994, 29, 585
[80] Leung C S Y, Wintreert-Fouquet M, Skellern D J. Switching time measurements of GaAs/AlAs and InGaAs/AlAs resonant tunnelling diodes. 1998 Conference on Optoelectronic and Microelectronic Materials and Devices, Proceedings (Cat. No. 98EX140), 2002, 144
[81] Kanaya H, Sogabe R, Maekawa T, et al. Fundamental oscillation up to 1.42 THz in resonant tunneling diodes by optimized collector spacer thickness. J Infrared, Millimeter and Terahertz Waves, 2014, 35, 425
[82] Izumi R, Suzuki S, Asada M. 1.98 THz resonant-tunneling-diode oscillator with reduced conduction loss by thick antenna electrode. 42nd International Conference on Infrared, Millimeter, and Terahertz Waves (IRMMW-THz), 2017, 1
[83] Sellai A, Raven M S, Steenson D P, et al. Double-barrier resonant tunnelling diode three-state logic. Electron Lett, 1990, 26, 61
[84] Sollner T C L G, Tannenwald P E, Peck D D, et al. Quantum well oscillators. Appl Phys Lett, 1984, 45, 1319
[85] Pfenning A, Hartmann F, Langer F B, et al. Cavity-enhanced resonant tunneling photodetector at telecommunication wavelengths. Appl Phys Lett, 2014, 104, 101109
[86] Pfenning A, Jurkat J, Naranjo A, et al. Resonant tunneling diode photon number resolving single-photon detectors. Proc SPIE 11128, Infrared Remote Sensing and Instrumentation XXVII, 2019, 1112808
[87] Watson S, Zhang W K, Tavares J, et al. Resonant tunneling diode photodetectors for optical communications. Microw Opt Technol Lett, 2019, 61, 1121
[88] Mutamba K, Flath M, Sigurdardottir A, et al. A GaAs pressure sensor with frequency output based on resonant tunneling diodes. IEEE Trans Instrum Meas, 1999, 48, 1333

Swagata Samanta received her PhD from Indian Institute of Technology Kharagpur (IIT Kgp). She continued her research as a postdoctoral fellow at the Indian Institute of Science (IISc), Bangalore and then at the University of Glasgow, UK. She is presently an Assistant Professor at SRM University, Andhra Pradesh, India. Her research interests include novel on-chip nanophotonic and nanoelectronic devices, integrated optics, neuromorphic circuits, VLSI systems, image/video processing, and artificial intelligence. She has authored and coauthored, as well as reviewed, several prestigious peer-reviewed papers that have been presented at international conferences and published in academic journals.